Computers & Geosciences 87 (2016) 101–111

Contents lists available at ScienceDirect

Computers & Geosciences

journal homepage: www.elsevier.com/locate/cageo

Case study

Improving assessment of geological structure interpretation of magnetic data: An advanced data analytics approach

Eun-Jung Holden [a,*], Jason C. Wong [a], Daniel Wedge [a], Michael Martis [a], Mark Lindsay [a], Klaus Gessner [b]

[a] Centre for Exploration Targeting, School of Earth & Environment, The University of Western Australia, 35 Stirling Hwy, Crawley, WA 6009, Australia
[b] Geological Survey of Western Australia, Mineral House, 100 Plain Street, East Perth, WA 6004, Australia

ARTICLE INFO

Article history:
Received 13 August 2015
Received in revised form
20 November 2015
Accepted 20 November 2015
Available online 2 December 2015

Keywords:
Data analytics
Magnetic data interpretation
Geological structure detection
Automated lineament detection

ABSTRACT

Geological structures are recognisable as discontinuities within magnetic geophysical surveys, typically as linear features. However, their interpretation is a challenging task in a dataset with abundant complex geophysical signatures representing subsurface geology, leading to significant variations in interpretation outcomes amongst, and within, individual interpreters. Previously, numerous computational methods were developed to enhance and delineate lineaments as indicators for geological structures. While these methods provide rapid and objective analysis, selection and geological classification of the detected lineaments for structure mapping is in the hands of interpreters through a time consuming process. This paper presents new ways of assisting magnetic data interpretation, with a specific aim to improve the confidence of structural interpretation through feature evidence provided by automated lineament detection. The proposed methods produce quantitative measures of feature evidence on interpreted structures and interactive visualisation to quickly assess and modify structural mapping. Automated lineament detection algorithms find the feature strengths of ridges, valleys and edges within data by analysing their local frequencies. Ridges and valleys are positive and negative line-like features detected by the phase symmetry algorithm which finds locations where local frequency components are at their extremum, the most symmetric point in their cycle. Edge features are detected by the phase congruency algorithm which finds locations where local frequency components are in phase. Their outputs are used as feature evidence through interactive visualisation to drive data evidenced interpretation.

Our experiment uses magnetic data and structural interpretation from the west Kimberley region in northern Western Australia to demonstrate the use of automated analysis outputs to provide: quantitative measures of data evidence on interpreted structures, and graphical evaluation of interpretation quality.

© 2015 Elsevier Ltd. All rights reserved.

1. Introduction

Geological interpretation of potential field data is a routine practice for structural analysis and is important for a wide range of industries including mineral exploration, CO_2 sequestration, groundwater, and geothermal energy industries. However, similarly to the interpretation uncertainty of seismic data (Bond et al. 2007), interpretation outcomes of potential field data are found to be highly variable amongst interpreters and lack consistency even within an individual (Sivarajah et al. 2013, 2014). To address this, there has been much effort in recent years to develop automated data analysis tools to facilitate fast and objective analysis of data. These tools are able to delineate specific feature characteristics within data using computational algorithms which perform mathematical filtering and/or pattern matching. For structural interpretation of magnetic data, various lineament detection techniques have been proposed (Blakely and Simpson, 1986; Hornby et al., 1999; Fedi, 2002; Cooper and Cowan, 2006; Cella et al., 2009; Holden et al. 2008, 2012).

The challenge however is in how to utilise and integrate automated analysis into the interpreters' workflow to improve the efficiency and robustness of interpretation outcomes. Automated analysis is based on data characteristics which may be associated with a variety of geological features and often result in a large number of false positives. Crucially, a purely computational approach does not consider geological feasibility and thus, does not guarantee a realistic interpretation. In the case of lineament detection, the detected lineaments may be associated with differing geological features such as faults, dykes, joints, igneous contacts, and unconformities. So while automated analysis is useful at least

* Corresponding author.
E-mail address: eun-jung.holden@uwa.edu.au (E.J. Holden).

http://dx.doi.org/10.1016/j.cageo.2015.11.010
0098-3004/© 2015 Elsevier Ltd. All rights reserved.

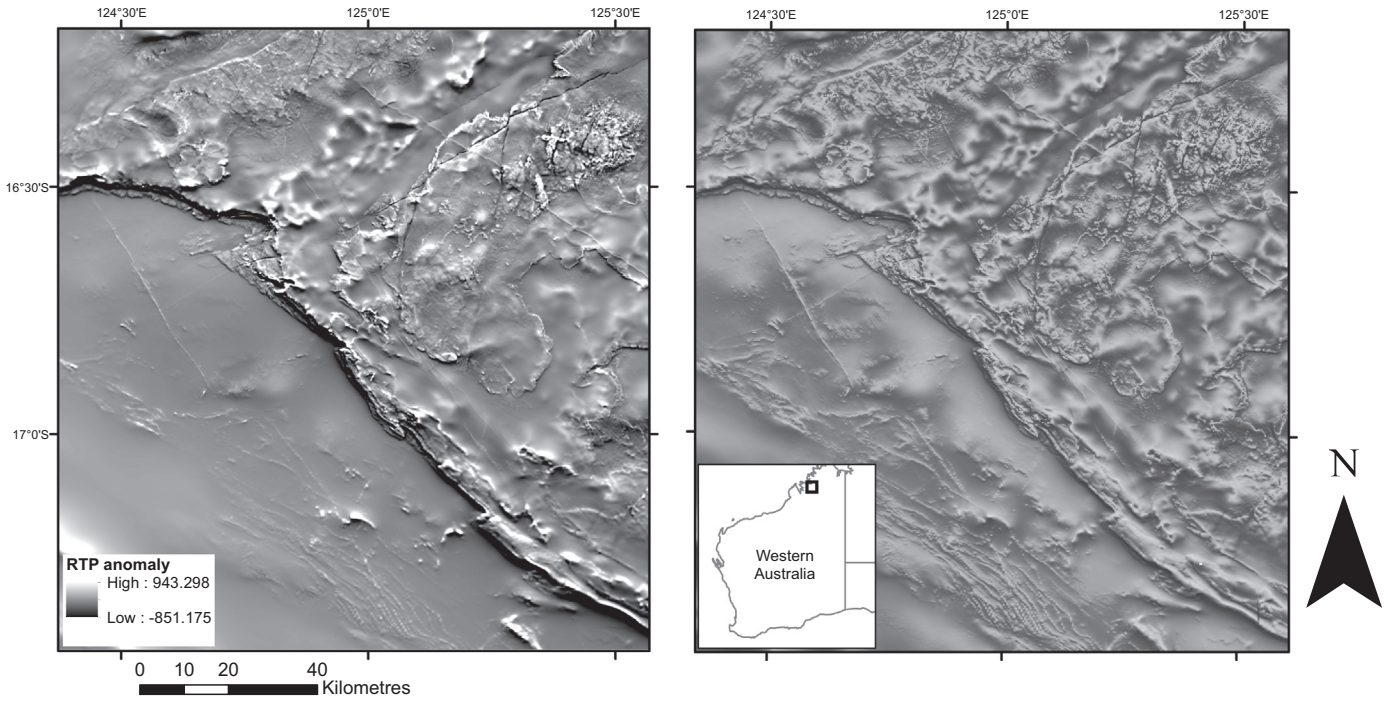

Fig. 1. (a) RTP (histogram equalised) and (b) PPDRC- filtered (with RTP as input) with a cut-off at 23 km or 271 cells (linear normalisation). The PPDRC filter enhances features in low-contrast areas.

as a first-pass analysis by providing features for further consideration, deciding on their selection and geological classification remains in the hands of an interpreter.

This study explores new data analytics methods which integrate automated lineament detection and interactive visualisation methods into interpreters' workflows to improve the confidence in structural analysis of potential field data. Automated lineament detection techniques, previously developed for potential field data analysis (Holden et al., 2010) are used in two specific ways to assist interpretation. In the first, they are used to generate a quantitative measure of confidence on interpreted lines based on automated data analysis results which will be referred to as feature evidence throughout this paper. Secondly, the confidence of mapped structures is assessed visually using an interactive visualisation interface which displays feature evidence over interpreted structures by manipulating colour display. This can also provide interpretation guidance as the interpreter traces a structure based on visual ridge/valley/edge characteristics in the geophysical data. Automated analysis highlights the same characteristics in the local neighbourhood to facilitate data supported interpretation.

Using potential field data and part of a larger subsequent structural interpretation from the west Kimberley region in northern Western Australia (Lindsay et al., 2015a), we demonstrate different ways to use automated analysis outputs to quantitatively or visually examine the quality of structural interpretation. Note that the data analytics methods presented in this paper are applicable to interpretation workflows for a wide range of geoscience images, such as satellite images and airborne photographic images, where linear features are sought for interpretation.

2. Interpreting geological structure from geophysical data

Structural geophysical interpretation was performed by Lindsay et al. (2015a) in order to better understand the crustal architecture and tectonic evolution of the region. Large-scale structures considered important for mineralisation and the extent of key rock units were defined as part of the interpretation. The interpretation was then used as input for mineral systems analysis aimed at determining prospectivity for a range of commodities (Au, Ni, and base metals) (Lindsay et al., 2015b). As such the interpretation was performed approximately between 1:250 000 and 1:500 000 map scale, which is appropriate to the resolution of the magnetic data.

The interpretation used in this case study was performed on magnetic data. A regional total magnetic intensity (TMI) grid was created by stitching together a series of regional surveys by the Geological Survey of Western Australia (GSWA) and other available open file surveys. Surveys were mostly flown with a line-spacing of 400 m, though some had a line-spacing of 200 m. Each survey was gridded to a 100 m cell size using the minimum curvature method prior to stitching. Some image processing techniques and filters were then applied to the stitched TMI grid. The reduction to the pole (RTP) filter is first applied to ensure that asymmetry in data are representative of source geometry or magnetic properties. Then a technique called phase-preserving dynamic range compression (PPDRC) (Kovesi, 2012; Holden et al., 2010) is applied to enhance structures. PPDRC combines high pass filtering and tone mapping techniques to enhance contrast in high dynamic range data such as magnetics. This technique is based on the principle that preservation of the phase component of signal in the frequency domain is critical for preserving feature characteristics in the image. PPDRC analyses local frequencies in the magnetic data in which high pass filtering can be applied by attenuating frequencies associated with wavelengths larger than a specific wavelength cut-off; then while preserving phase, it applies a range reduction function to the amplitude in the frequency domain. Then the phase and re-mapped amplitude are combined to reconstruct the enhanced grid data.

The outputs from the RTP and PPDRC (run on the RTP output) filters are shown in Fig. 1. For PPDRC, we used a large wavelength cut off at 23 km (271 cells) for high pass filtering to ensure that most features are preserved while their contrast is enhanced. Phase based feature detection techniques, which will be described

in Section 3, are a form of high pass filtering, but PPDRC is used to enhance feature contrast for interpretation, similarly to the use of histogram equalisation. Note that while our study used these specific pre-processing filters, the workflow to validate and enhance the robustness of interpretation presented in this paper is not limited to these, and is applicable to other filter responses such as upward continuation to map structures at a specific depth, or high pass filters such as vertical derivatives and automated gain control.

The interpretation used several sources of geological information to augment the geophysical data. The primary constraints were the GSWA 1:250 000 map sheets YAMPI (SE 51-3) and CHARNLEY (SE 51-4). Outcrop information was obtained from GSWA's WAROX database of structural measurements and field observations in order to provide structural constraint on the orientation and type of foliations, and the trend and plunge of fold axes.

Two distinct parts of the case study area can be discerned from the geology and geophysics. Tyler and Griffin, 1990 identify the southern part of the area as the Palaeoproterozoic King Leopold Orogen comprising mostly granitoid rocks cross-cut by a series of mafic dykes. Some metaturbitic rocks are intruded by mafic intrusive rocks. The granitoids display a relatively low amplitude, smooth geophysical response, whereas the mafic dykes can be interpreted from long and linear features of relatively high amplitude. Some of these features are quite subtle, and interpretation benefited from the use of PPDRC.

The northern part of the area contains the Kimberley and Speewah basins, which are a series of sedimentary and mafic volcanic and mafic intrusive units that are moderately deformed into open, regional-scale folds (Tyler and Griffin, 1990). The sedimentary layers are characterised by a low amplitude magnetic response, whereas the mafic volcanic and intrusive units (the Carson Volcanics and Hart Dolerite respectively) have a distinctive high amplitude, high frequency response. Faults and folds have been interpreted from the area. The boundary between the Kimberley and Speewah basins and the King Leopold Orogen is marked by a geologically complex region of Kimberley and Speewah basin units thrust up against the King Leopold Orogen (Tyler and Griffin, 1990).

This interpretation by Lindsay et al. (2015a) uses potential field data as the primary dataset, and other datasets for support. Previously, the Geological Survey of Western Australia (GSWA) produced the 1:500 000 scale structural dataset (Martin et al., 2014) which was primarily compiled from multiple editions of 1:100 000 and 1:250 000 GSWA Geological series maps, and GSWA and Geoscience Australia (formerly AGSO, formerly BMR) 1:250 000 and 1:1 000 000 regional geological maps. Some modifications have been made where additional datasets (for example, magnetics, radiometrics, gravity, remote sensing, drilling and recent field mapping) were available. Note that the Lindsay et al. (2015a) interpretation approach focussed on identifying deeper crustal features as well as those at or close to the surface. The scale of the two datasets is not exactly equal, as the Lindsay et al. (2015) interpretation was performed between 1: 250 000 and 1:500 000 scale and shows more detail in some areas. Fig. 2 shows the structure map of Lindsay et al. (2015a) and the GSWA structure map in (a) and (b) respectively.

3. Automated lineament detection

There are three types of features in magnetic data which are useful for structural analysis, namely: ridges and valleys for positive and negative anomalies respectively which are particularly useful in tracing dykes and structures; and edges (displaying an asymmetric signal) for anomaly boundaries which are useful in identifying geological contacts and faults. All of these features are associated with the term lineaments or anomalies within magnetic data, but their use may vary depending on the task. For example, ridges may indicate the presence of a magnetically susceptible mafic dyke, valleys could indicate a fault and edges may indicate the boundary between rock types with contrasting petrophysical values.

This study detects lineaments using two generic image feature detection techniques: phase symmetry (Kovesi, 1997) and phase congruency (Kovesi, 1999). These techniques were previously applied to magnetic data (Holden et al., 2008, 2010, 2012; Aitken et al., 2013) and other geoscience datasets (Vasuki et al., 2014).

For structural interpretation of geophysics data, the features of interest are step-like features which are referred as edges in this manuscript, or line-like features where lines brighter/darker than its surrounding are referred as ridges/valleys. These features are closely associated with the properties of the local frequency components of the signal. Where a Fourier transform is commonly used to examine periodicity over an entire signal by decomposing

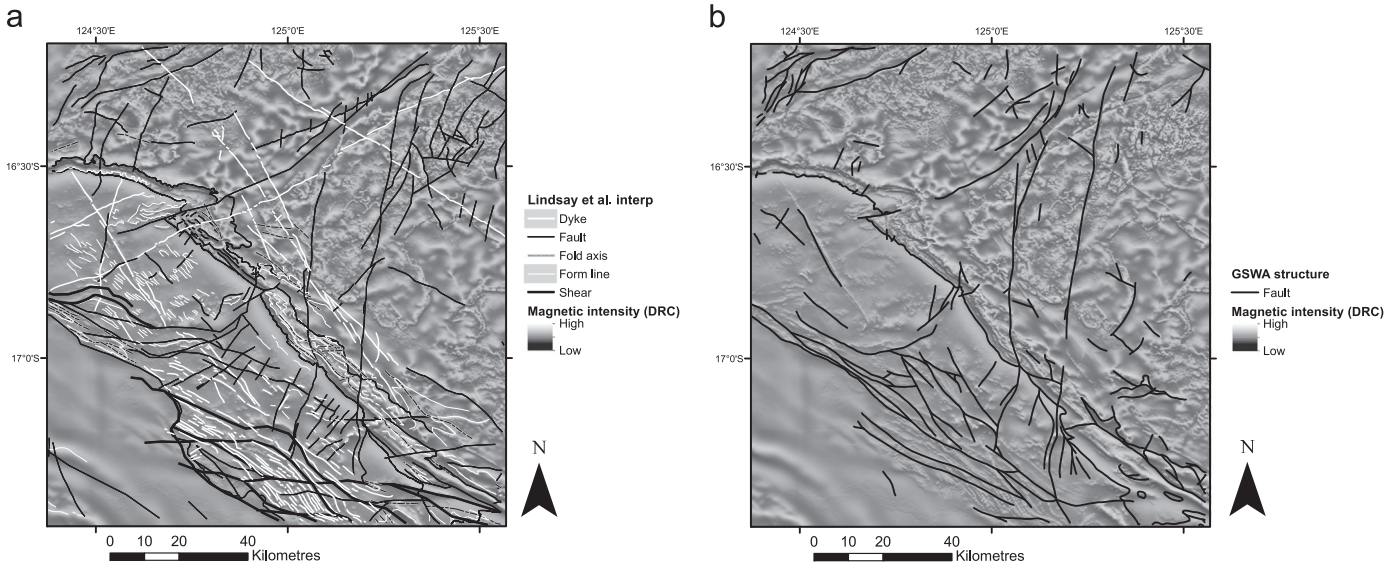

Fig. 2. Structure interpretation by Lindsay et al. (2015a) shown in (a) over RTP-PPDRC filtered output; and GSWA structure map is shown (b) over RTP-PPDRC filtered output.

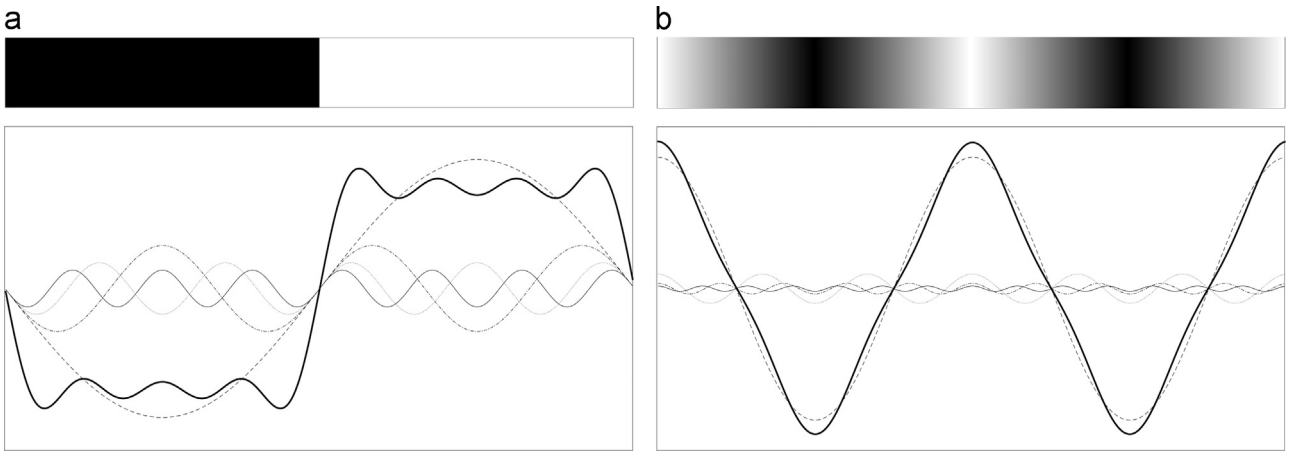

Fig. 3. The top row shows two example profiles of grid data: (a) a step edge and (b) valley-ridge-valley features. These waveforms can be decomposed into their Fourier series and the first few terms of the respective Fourier series are plotted as dotted lines, and their sum as the solid line (adapted from Kovesi, 1999).

the signal into a set of sinusoids with various phases, wavelengths and magnitudes, the local frequency components capture the properties of a signal at a given grid point. Fig. 3(a) shows a step feature where a profile line from the grid goes from low to high (or dark to bright as shown in the bar); the frequency components extracted from this profile line at various scales are shown as dotted lines in the plot. We can see that at the point where the signal changes from low to high, all of the frequency components are in phase, i.e. they are all at the same point in the sinusoidal cycle. This demonstrates that edge features are characterised in the frequency domain by the local frequency components being in-phase (i.e. congruent). Fig. 3(b) illustrates another example containing ridge (bright) and valley (dark) features in the profile line. The figure shows symmetric features, i.e. the ridges and valleys are axes of symmetry where all of the local frequency components are at their extreme points.

Here we briefly provide an overview of the implementation of the phase symmetry and phase congruency algorithms; further technical detail is provided by Kovesi (1997), (1999). The phase symmetry and phase congruency algorithms are based on analysing the phase component of local frequency of the signal computed at every grid location. The local frequency is calculated using a wavelet transform technique, where banks of filters are constructed at a number of scales. In the implementation, the wavelength of each successive scale is double the previous scale. At each scale, filters are constructed in quadrature-pairs, i.e. an even-symmetric (cosine) wavelet and an odd-symmetric (sine) wavelet, each modulated by a Gaussian. By convolving the data with a quadrature pair of filters at a specific location, we obtain the responses for the even and odd symmetric filters at a particular scale, which can be combined by considering these as a 2D-vector with the magnitude representing the response amplitude at that scale and the vector orientation representing the phase of the local frequency. Thus, this approach adapts and extends the approach proposed by Morlet et al. (1982). In practice, the convolution is performed efficiently in the frequency domain via the Fourier transform, where the resulting complex values simultaneously encode the even and odd symmetric responses in the real and imaginary components respectively. Here we use them for phase analysis.

The phase symmetry algorithm (Kovesi, 1997) finds ridge and valley features by identifying the locations where all of the frequency components are most symmetric in their cycle. Symmetry occurs when the magnitudes of the even symmetry filter responses are large and the magnitudes of the odd symmetry filter responses are small for all scales within the band of frequencies.

Given $e_n(x)$ and $o_n(x)$ which are the even and odd filter responses respectively at scale n at a grid location x, symmetry is quantified by subtracting the magnitude of the odd symmetry filter output, $|o_n(x)|$, from the magnitude of the even symmetry filter output, $|e_n(x)|$, with the differences summed over all scales; a noise threshold T is then subtracted and any resulting negative values (corresponding either to noise or asymmetric responses such as edges) are set to 0. The resulting value is normalised by the sum of the magnitudes of these response vectors where magnitude of a vector at scale n, at a grid location x is defined by $A_n(x)=\sqrt{e_n(x)^2 + o_n(x)^2}$, resulting in the symmetry outputs being a contrast invariant quantity ranging from 0 (no symmetry) to 1 (maximum symmetry). Thus phase symmetry is defined as:

$$\mathrm{Sym}(x) = \frac{\Sigma_n \lfloor \lceil |e_n(x)| - |o_n(x)| \rceil - T \rfloor}{\Sigma_n A_n(x) + \epsilon} \quad (1)$$

where the $\lfloor\rfloor$ operator sets the enclosed value to 0 if it is negative otherwise it preserves the enclosed value, and ϵ is a small constant to prevent division by zero. Additionally, the sign of the even filter symmetry responses can be used to classify a symmetry feature as a ridge (for positive values) or valley (negative values).

In magnetic data, the magnitude of a feature relative to the

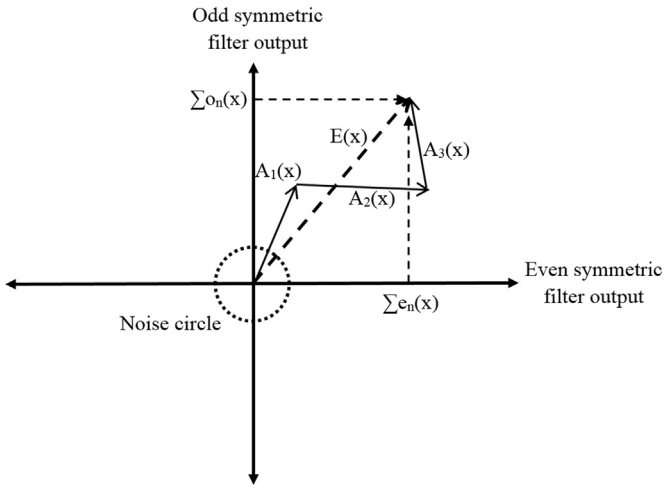

Fig. 4. The even and odd symmetric filter responses from different scales are plotted as solid vectors head to tail, and their sum given by the dashed vector $E(x)$. The magnitude of $E(x)$ is the local energy; the phase congruency response is the ratio of this length to the total path length taken by all of the solid vectors representing the filter responses for each scale.

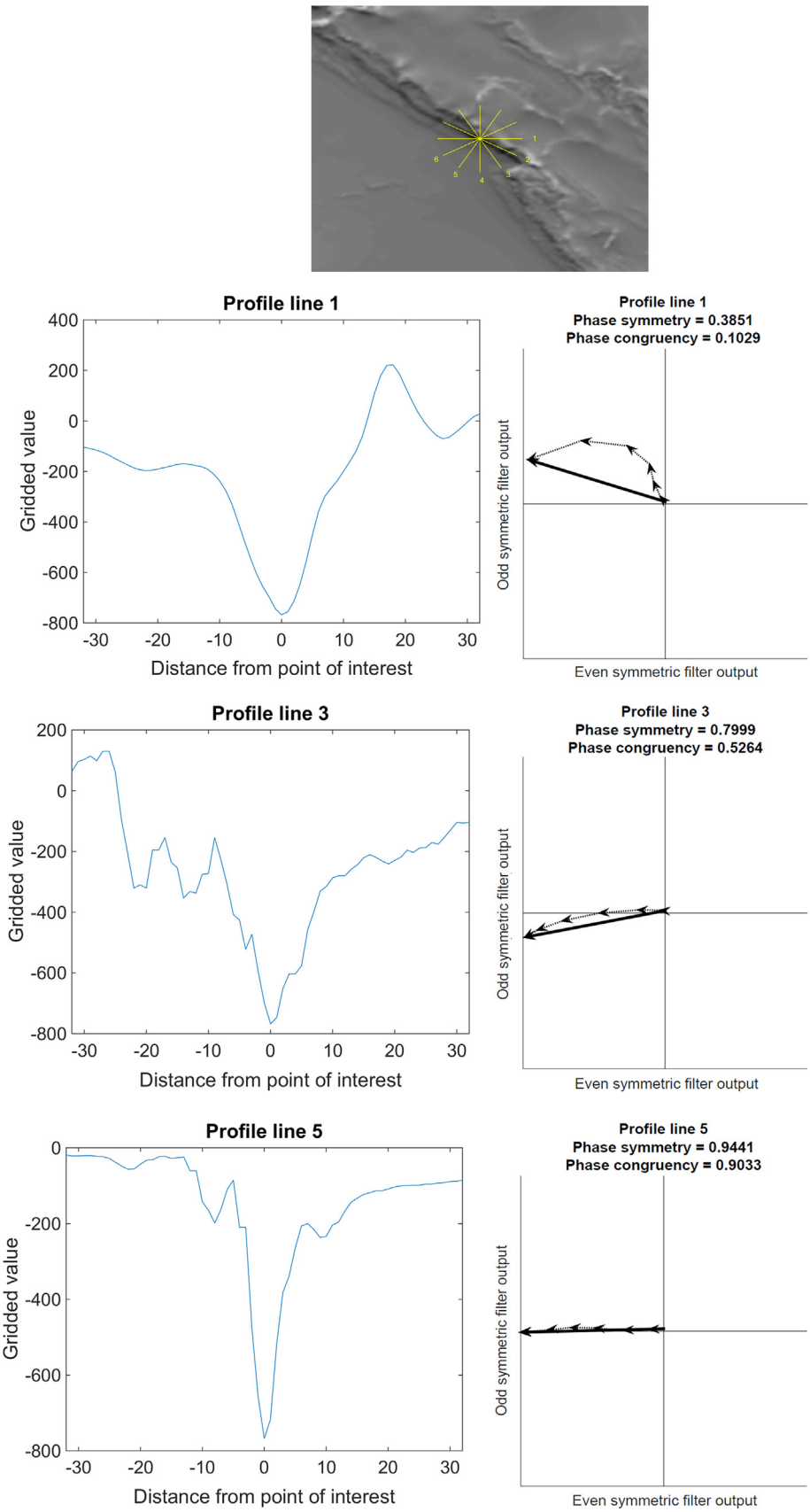

Fig. 5. A demonstration of phase congruency and phase symmetry by visualising the filter responses at for profile lines taken at different orientations (top). The dotted arrows on the graphs indicate the filter responses at each scale for a given orientation; responses are ordered from longest wavelengths (innermost components) to the shortest wavelengths (outermost components); the phase congruency measure shown is the ratio of the magnitude of the solid vector (i.e. the sum of the filter responses) to the length of the paths taken by the individual filter responses. The rightmost point of the profiles in the graphs correspond to the labelled ends of the corresponding profile lines overlaid on the grid. Combining the responses over all orientations, the overall phase symmetry response is 0.5988 and the phase congruency value is 0.4049. (The reader is referred to the web version of this article for coloured figures.)

signal strength may be very small, thus the contrast invariant feature strength provided by phase symmetry is advantageous compared to other widely used linear feature detection algorithms which are based on feature contrast strength, such as the Hough transform (Gonzalez and Woods, 2002).

The above explanation considers only profile lines in 1D. To apply phase symmetry to a 2D grid, we create a bank of log-Gabor filters at six orientations. Then the phase symmetry is computed similarly using the outputs of all filters at all orientations θ, i.e.:

$$\mathrm{Sym}(x) = \frac{\Sigma_\theta \Sigma_n \left\lfloor \left[|e_{n,\theta}(x)| - |o_{n,\theta}(x)| \right] - T \right\rfloor}{\Sigma_\theta \Sigma_n A_{n,\theta}(x) + \epsilon} \quad (2)$$

Later, in Fig. 5, we demonstrate that ridge and valley features often exhibit symmetry in many orientations, not just perpendicular to the orientation of the feature.

The phase congruency algorithm (Kovesi, 1999) finds edge features by identifying the locations where the frequency components are in phase at all scales, i.e. the quadrature pairs of filters for each band of frequencies have the same or similar phase angles, and filter responses of similar magnitude for all scales. This is evident when visualised by plotting the even and odd symmetric filter outputs as components of a vector on orthogonal axes as shown in Fig. 4, in which case the phase is given as the vector orientation – the solid vectors show the filter outputs for each scale. Firstly, the local energy of the signal is defined as the magnitude of the sum of the filter responses at each scale, i.e. the magnitude of the dashed vector E(x). Then, phase congruency is calculated from the local energy, divided by the sum of the magnitudes of the filter responses at each scale, that is $A_n(x)$ as previously described for phase symmetry and where each filter response is weighted to ensure that congruency is evenly distributed over the range of scales. Again, this quantity ranges from 0 (no congruency, i.e. the filter response vectors at each scale cancel out perfectly) to 1 (perfect phase congruency, i.e. the filter responses have identical phases at all scales and identical energy magnitude at each scale), which would be represented as vectors of identical magnitude and orientation in Fig. 3. Mathematically (Morrone and Burr, 1988; Morrone and Owens, 1987):

$$PC(x) = \frac{|E(x)|}{\Sigma_n A_n(x)}. \quad (3)$$

Noise within data will result in the filter responses being small in value and having random phase values. We handle noise by identifying locations where $E(x)$ lies within some radius from the origin, shown by the dashed circle in Fig. 4, and setting the phase congruency values to 0 at these locations.

In extending phase congruency to 2D, an extra step is required to handle variations in phase with orientation, not required when extending phase symmetry to 2D. This is because the phase information at a point will vary with the orientation of the profile line (e.g. profile lines across a step change may go from low to high values, or high to low values depending on the orientation of the profile line). An approach based on classical moment analysis equations is used where phase congruency is firstly computed independently for each orientation. Then, at each location the maximum and minimum moments are computed integrating the phase congruency values from all orientations at that location, again the moments range from 0 to 1. In addition, a weighting factor is also included to ensure that responses of similar magnitude are observed at each scale, which incorporates a measure of contrast invariance.

3.1. Phase responses in magnetic data

In practice we use the locations with high phase symmetry for locating ridges and valleys, and the locations of high phase congruency for detecting edges. An example is presented in Fig. 5, where profile lines are taken at six orientations across a valley. For each profile line, the corresponding odd and even filter responses for 6 scales, starting with a minimum wavelength of 3 cells, are shown and plotted. In this example, the phase congruency (i.e. ratio of the length of the solid vector to the lengths of the dotted component vectors) is high for all orientations. All profile lines cross this valley with the exception of profile line 2 which runs along it, and they produce a symmetric profile regardless of the orientation. Therefore it is sensible to compute phase symmetry using filter responses for multiple orientations as in Eq. (2) above.

In the example in Fig. 5, as it is a point of symmetry we expect that the even filter responses will have large negative values, with negligible odd filter responses. This is largely reflected in the filter responses shown in Fig. 5, where this is strongly demonstrated for profile lines 3 and 5. Of course, as geophysical features do not occur in isolation, the phase symmetry algorithm will not always give such perfect responses, e.g. as shown in profile line 1, the odd filter responses are non-negligible so the phase symmetry value decreases. Note however, that when considering the responses at all orientations, the overall result is that this is a point of symmetry.

Also note the phase congruency values for this same location. Although we have described phase congruency as being most useful for detecting edges, this example demonstrates that it also produces strong responses for ridge and valley features, as illustrated by the similar orientations of the vectors for each scale on the 2D plots.

4. Quantifying and visualising feature evidence of interpretation

The phase based methods described in this paper are applicable to any grid data, in its original or filtered output, on which the interpretation is drawn. In this study, we applied these phase based feature delineation techniques to a magnetic grid which is processed using the reduction to the pole (RTP) filter and dynamic range compression (PPDRC) (Kovesi, 2012; Holden et al., 2010) filters.

Structural interpreters may utilise feature evidence based on feature strength provided by phase symmetry and phase congruency in two different ways. One is to generate a quantitative measure of feature evidence on the structures which are being mapped; and the other is to use their feature strength to guide the mapping of structures through interactive visualisation. For this experiment, we used the structure map of Lindsay et al. (2015a) and the GSWA structure map, which were previously discussed in Section 2.

4.1. Quantitative measure of feature evidence

Feature evidence is based on the ridge, valley and edge strengths of the RTP-PPDRC processed grid previously shown in Fig. 1(b). Fig. 6 shows the ridge and valley strengths of the grid calculated from the phase symmetry algorithms in (a) and (b) respectively, and edge strength from phase congruency in (c).

Structural interpretations by Lindsay et al. (2015a) and GSWA (Martin et al., 2014) which were shown previously in Fig. 2 are used to assess their feature evidence. Feature evidence is quantified by aggregating the feature strength (i.e. phase symmetry or phase congruency output) along a mapped structure, which is then normalised by the length. Although the feature evidence outputs range between 0 and 1, it is unreasonable to expect structures with strong data evidence to produce symmetry or

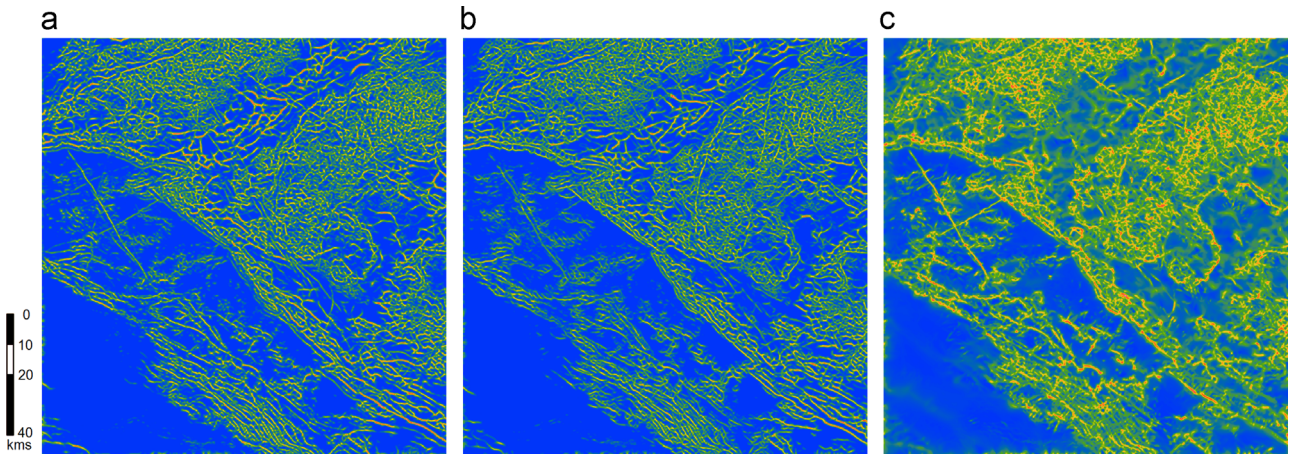

Fig. 6. (a) Ridge strength from phase symmetry; (b) valley strength from phase symmetry; and (c) edge strength from phase congruency, using the RTC-PPDRC filtered grid in Fig. 1(b). Phase symmetry was calculated using a minimum wavelength of 3 cells, with 3 scales and a multiplier of 2.1. Phase congruency was calculated using a minimum wavelength of 3 cells, 6 scales, with a multiplier of 2.1. Both phase algorithms produce a value between 0 and 1, and an isoluminant rainbow colour map of blue to pink is used for display. (The reader is referred to the web version of this article for coloured figures.)

congruency responses above about 0.3. This is because realistic data with noise will never exhibit large areas containing the kind of theoretically-perfect symmetry or congruency required to produce high-end filter responses. Hence, we report the cube root of the filter output when displaying numerical feature evidence values. As each filter produces values between 0 and 1, an application of the cube-root function provides a transparent kind of "data stretch" to boost filter responses. This transform also helps to offset human bias – increasing seemingly-low evidence values like 0.3 to values more representative of their importance.

An experiment was conducted by comparing feature evidence measures on different types of structures, namely dyke, fault, fault axis, form and shear zones from the interpretations GSWA and Lindsay et al. (2015a). Their feature evidence values are calculated from three feature types, ridge, valley and edge, using RTP and RTP-PPDRC filtered grid using the wavelength cut-off value of 271 cells (23 km). Note that the aim is not to show that one dataset is more accurate, better or more useful than the other, rather that different approaches in producing geological datasets and scale of study can be measured with the feature evidence analysis described here.

The results in Table 1 show the mean feature evidence measures for different structure types, feature types and input datasets for feature detection. It is important to note that edge evidence values are not to be directly compared with ridge/valley evidence values as phase congruency and phase symmetry estimate different quantities.

In ridge/valley evidence, it is also notable that faults are better evidenced by valley strength, than ridge strength. This reflects the fact that faults typically appear as negative linear anomalies in aeromagnetic surveys due to magnetite destruction in the faulting process. In contrast, dyke and form features are better evidenced by ridge strength than valley strength, which shows that they are more likely to appear in positive linear features than faults, which is generally the case.

In addition, for the same feature type (ridge, valley and edge), evidence on each structure type only vary slightly for different input datasets. These input datasets included RTP and RTP-PPDRC (with wavelength cut-off at 23 kms). The result shows that while ridge and valley evidence did not have noticeable change with PPDRC enhancement, edge evidence had some improvement, mostly greater than 5% and less than 10%. This may be associated with some level of noise removal applied by PPDRC, contributing to a more robust edge detection result by the phase congruency algorithm.

4.2. Interactive visualisation of feature evidence

An efficient way to improve interpretation confidence is to check feature evidence on interpretation through interactive visualisation. However, it is not a trivial task to present this feature evidence effectively, whilst ensuring minimal interruption to the interpreters' viewing of the magnetic data (TMI or other filtered data) on which the interpretation is being performed. Current GIS tools commonly used allow multiple data to be displayed through either transparencies or switching on and off the overlaying data. Recently, an interactive multi-data display method called image blending has been proposed for geoscientific data (Kovesi et al., 2014). This study extends this concept to allow interactive visualisation of feature evidence on interpreted structures. The challenge in this integrated display is to ensure that the data being interpreted and the feature evidence layer are easily distinguishable, comparable and contrastable. Two types of visualisation methods are suggested: the field of view (FoV) based visualisation;

Table 1
Comparison of feature evidence values across ridge, valley, and edge evidence mean values from feature evidence analysis on the RTP filter output; and RTP-PPDRC where PPDRC is applied with a cut-off at 271 cells (23 km). Note these values are the cube roots of the calculated evidence values.

Structure	Interpretation	Group-count	Ridge evidence mean		Valley evidence mean		Edge evidence mean	
			RTP	RTP-PPDRC	RTP	RTP-PPDRC	RTP	RTP-PPDRC
Dyke	Lindsay et al.	234	0.402	0.431	0.312	0.332	0.465	0.505
Fault	GSWA	312	0.295	0.300	0.304	0.304	0.408	0.438
Fault	Lindsay et al.	190	0.309	0.313	0.364	0.376	0.443	0.471
Fold_axis	Lindsay et al.	42	0.332	0.344	0.315	0.323	0.415	0.451
Form	Lindsay et al.	245	0.330	0.361	0.280	0.296	0.415	0.449

and the vector based visualisation. Both of these visualisation techniques use a common data overlaying method which controls the chromaticity and luminance of colour to display the feature evidence and geophysics data which is being interpreted.

4.2.1. Data overlaying method

Our data overlay method uses hue to represent the feature evidence layer, and intensity to represent the underlying magnetic data from which the feature was extracted. This method differs from a simple linear interpolation which conflates features from two datasets, due to our relatively independent perception of hue and brightness: features in geophysical data appear as patterns in brightness, while features in feature evidence data appear as patterns in hue. Features of each type are maximally distinguishable when colourisation does not affect the perceived brightness of any point, i.e. when the selected confidence colourmap consists only of isoluminant colours. The presence of varying-luminance colours in the colourmap creates false anomalies when visualising confidence, with regions of darker confidence colour spuriously appearing to have low geophysical response. As such, our visualisation methods only use isoluminant colour maps to represent feature confidence.

Further, our interactive visualisation allows interactive control of the level of opacity in rendering of the feature evidence layer from completely hiding the underlying data to showing just the underlying data being displayed without the feature evidence layer (Fig. 7). This interactivity extends the current functionality on switching on and off layers in a GIS environment.

The data overlay method output is determined by a colourised feature evidence overlay modulated at each point by the strength of the underlying geophysical data. Ideally, each point's luminance should be determined solely by the geophysical value recorded at the point, and each point's chrominance should be determined solely by the feature evidence value calculated for the point. That is, bright points should identify strong responses in the underlying geophysical data, and points of "hot" hue (if using a heat colourmap) should identify strong feature evidence. In practice, this effect can be achieved by (pointwise) multiplying a greyscale rendering of the geophysical data with the colourised feature data evidence information.

More specifically, suppose that $V{:}A \to [0,\ 1]$ is a map from some point set A to geophysical data values, and that $C{:}B \to [0,\ 1]$ is a similarly defined map of feature evidence levels. Furthermore, let $P{:}[0,\ 1]\to[0,\ 1]^3$ be a map from possible feature evidence levels to their corresponding colours (with colours here represented as vectors of real numbers between 0 and 1 inclusive). We define the map $M{:}\ A \to [0,\ 1]^3$ taking each point of V to its modulated colour as follows:

$$M(p) = \begin{cases} V(p)(1,\ 1,\ 1) & \text{if } p \notin B \\ V(p)P(C(p)) & \text{if } p \in B \end{cases} \tag{4}$$

That is, points are colourised according to the colour of their associated confidence level (if such a value exists), and darkened according to the level of their associated geophysical reading.

This data display method is suboptimal, however, when important features are located in low-intensity regions of a geophysical data set. This can occur, for instance, when a user is looking to identify features that lie in "valleys" of geophysical response. As it is difficult to perceive the hue of low-luminance colours, the user will receive little or no information from the confidence overlay. To account for this situation, we allow the user to quickly invert the luminance of the geophysical data set (that is, set high-response regions to dark shades, and low-response regions to light shades). Such an inversion facilitates the clear display of the confidence overlay in low-response areas. An example of the inversion of the luminance is shown in Fig. 8.

Interactive user control determines the influence of feature evidence information on their interpretation in our interface by "diluting" the overlay with some amount of geophysical data. This is achieved using the standard weighted sum approach. More specifically, take V and M defined as above, and $\lambda \in [0,\ 1]$ as an "influence" factor for feature evidence colours (with $\lambda = 0$ giving no confidence influence and $\lambda = 1$ giving full influence). We define a new map $M'{:}A \times [0,\ 1]\to[0,\ 1]^3$ giving the colour of a point $p \in A$ with influence factor $\lambda \in [0,\ 1]$, as follows:

$$M'(p,\ \lambda) = \lambda\, M(p) + (1 - \lambda)\, V(p)\,(1,\ 1,\ 1) \tag{5}$$

Notice that setting $\lambda = 0$ displays only the original data set, setting $\lambda = 1$ displays the modulated confidence overlay as defined by M, and setting λ to any intermediate value linearly interpolates between these two extremes.

4.2.2. Field-of-view based visualisation

This visualisation method allows interpreters to view the circular area within the specified radius which will be referred to as the field of view (FoV). The centre of FoV is tied to the position of the mouse cursor, as shown in examples in Fig. 9. The interpreter can also modify the radius of FoV and the opacity of the feature evidence layer.

The FoV based visualisation may be useful to guide the mapping process of a specific structure, but is also useful in identifying regions of data with high feature evidence to ensure objective analysis of data. Previously, Sivarajah et al. (2014) showed that an

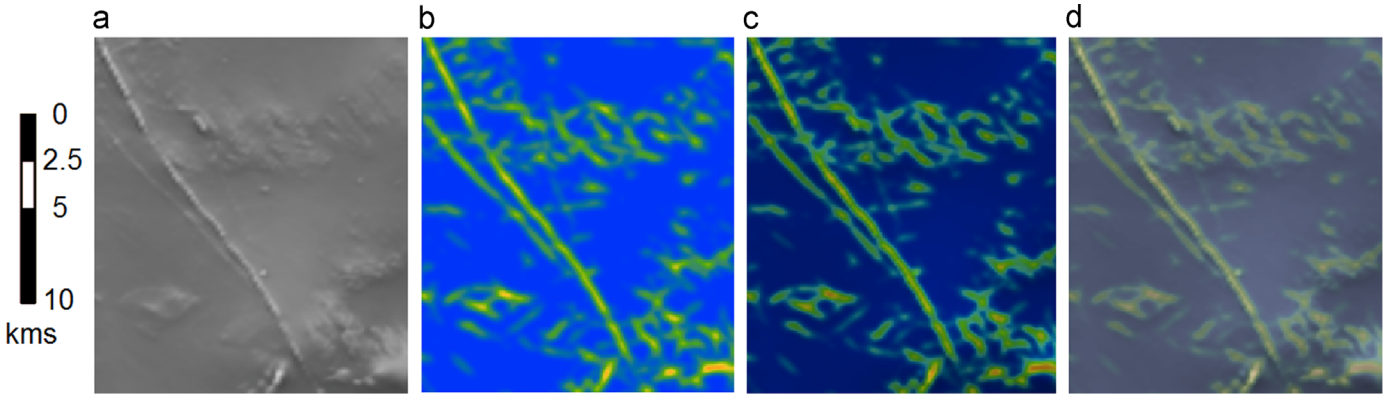

Fig. 7. (a) RTP data; (b) ridge strength; (c) a combined display of ridge strength (represented in colour) and RTP data (represented in intensity) with the opacity level 1; and (d) a combined display of ridge strength (represented in colour) and RTP data (represented in intensity) with the opacity level 0.3. (The reader is referred to the web version of this article for coloured figures.)

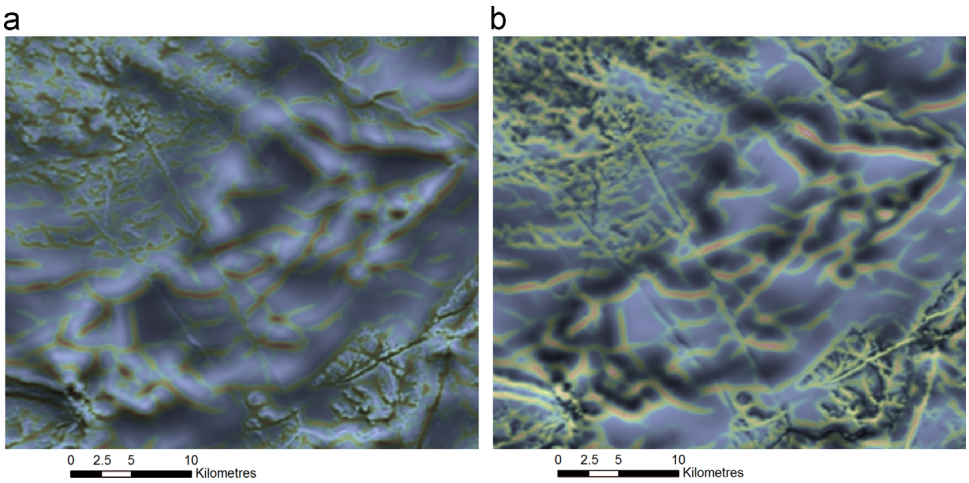

Fig. 8. An example of the usefulness of inverting the luminance, highlighing strong feature evidence in low-intensity areas. The valley feature evidence is shown using the data overlaying method with normal luminance in (a) and with inverted luminance in (b). (The reader is referred to the web version of this article for coloured figures.)

interpreter's visual attention in magnetic data is drawn to the features with high contrast in intensity, colour and orientation to their surroundings. The use of contrast invariant feature evidence provided by phase congruency and symmetry to assist interpreters' search for geological features will address this challenge as features in magnetic data may not present in high contrast to the surroundings.

Interactive user control of the location, radius and opacity of the FoV allow interpreters to access feature evidence in modifying interpreted structures or drawing new structures by shifting the feature evidence information to match the scope and position of their attention.

4.2.3. *Vector based visualisation*

This is a visualisation method to display feature evidence over existing, mapped line features. When in this mode, the vector line features are rendered as thick lines (rectangular sections) which act as a window through which the user can view restricted sections of feature confidence (using the data overlaying method shown in Fig. 7). Fig. 10 shows the interpreted lines whilst visualised in this mode. This method is intended primarily as a spell-check for feature lines; a user can enable the vector visualisation mode after having completed an interpretation, and receive immediate visual feedback (in the form of polygons revealing "hot" or "cold" areas) on feature evidence along the structure lines they have drawn. Through this feedback, a user can then see where their lines begin to deviate from the strongest feature evidence, and the direction in which they may wish to adjust their interpretation. It allows interactive control on the width of the lines to specify the size of the neighbourhood on which feature evidence is viewed. When a line is being actively moved (either during the original placement of a line or in subsequent position adjustments), the vector based confidence visualisation is updated interactively as the line's position is changed. As with the FoV base visualisation, both the opacity of the evidence layer as well as the line widths can be adjusted by the user in real-time.

5. Conclusions

The paper presents an innovative data analytics method to improve confidence on structural interpretation of magnetic data by harnessing the power of automated feature detection and interactive visualisation. The interpretation support is built upon relationships between data evidence and interpreted structures, providing at its most basic level the geological equivalent of a spell checker. Automated lineament detection techniques analyse the evidence of features, specifically ridges, valleys and edges. Their feature strengths are used to provide evidence on interpreted

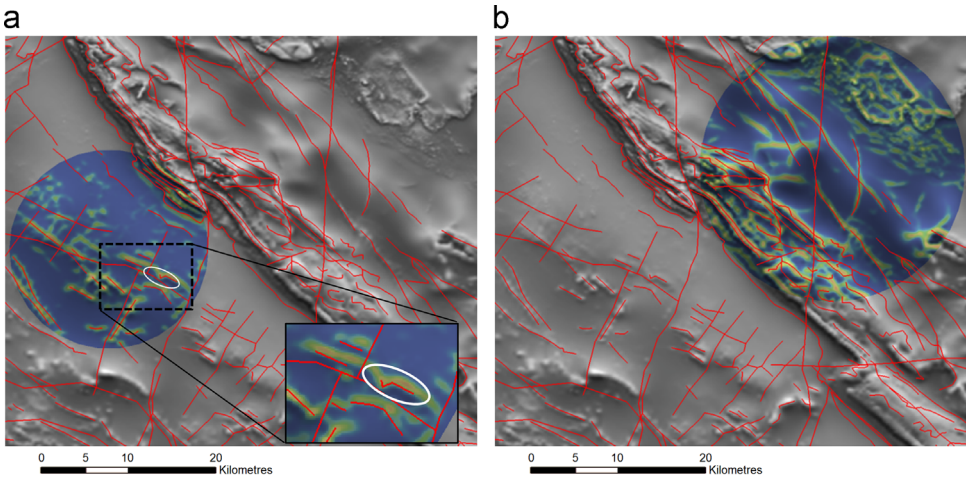

Fig. 9. Two examples of the FoV data overlay visualisation method, with the circular position controlled via the mouse cursor, with additional controls for opacity of the feature evidence layer, as well as area radius size. The inset in (a) shows the evidence of interpreted structure continuing beyond the annotated line. (The reader is referred to the web version of this article for coloured figu

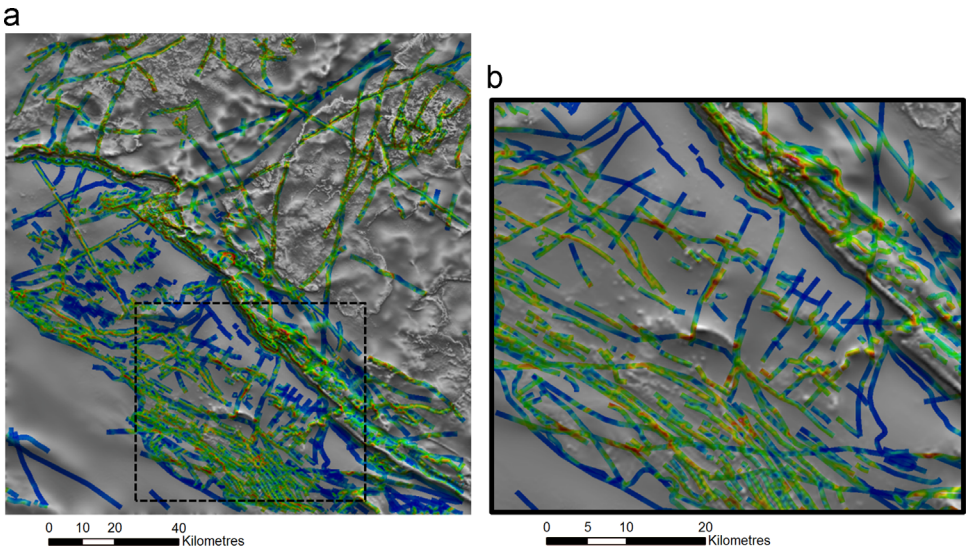

Fig. 10. Example of the vector-based visualisation which provides an at-a-glance view of the feature evidence supporting interpretation: (a) the edge feature evidence with non-inverted data luminance; and (b) a closer view of the area indicated by the dashed box in (a). Note that the data luminance can be inverted, as shown in Fig. 8. (The reader is referred to the web version of this article for coloured figures.)

structures. Two different methods are proposed: one is quantified feature evidence measures on interpreted structural interpretation, and the other is interactive visualisation of feature evidence over the interpreted map by controlling colour and intensity of the display to allow visual validation of the interpretation based on their data evidence.

Using the magnetic data from the Kimberley region of northern Western Australia and two different structural interpretations, an experiment was conducted to quantify the feature evidence on different types of structures. The results show that these measures align with their appearance characteristics represented by different types of features (i.e. ridge, valley and edge), with edge strength being the most reliable feature evidence measure. We also showed that enhanced grids using RTP-PPDRC filters provide slightly higher feature evidence measures than RTP-only filtered output, warranting the use of a suitable enhancement technique for feature evidence quantification. In addition, interactive visualisation techniques are developed to quickly and visually assess interpretation. They are based on a display method which overlays feature strengths on magnetic data using colour and intensity of the display. Two types of visualisation techniques are proposed: one allows the viewing of feature evidence through interactive control on viewing location and opacity of feature evidence; the other allows an at-a-glance overview of feature evidence over all of the interpreted structures by displaying the feature strength along interpreted lines. Although our data analytics approach is applied to magnetic data interpretation, the concept of using automated analysis as feature evidence to improve the quality of image interpretation is widely applicable beyond magnetic surveys and even geoscience itself.

5.1. On-going development

A number of improvements are being made to the proposed methodology. The first is to improve the scope of quantified confidence on interpreted structures by integrating feature evidence from multiple datasets which are often used as complementary datasets for interpretation, such as gravity combined with magnetics. Our on-going research focuses on developing a methodology to effectively integrate feature evidence from different datasets. The second is to develop a workflow to utilise the proposed feature evidence measure to minimise/define uncertainty in 3D models. Previous works on 3D model uncertainty analysis (Lindsay et al., 2012, 2013; Wellmann, Regenauer-Lieb, 2012) have identified that understanding uncertainty within interpreted input data, prior to model integration, is key to understanding the effects of uncertainty in geological modelling. We aim to use the feature evidence measure in building a 3D modelling workflow to minimise and quantify interpretation uncertainty and evaluate their effectiveness in improving the integrity of 3D models. The third planned improvement is to develop methodologies to support lithology interpretation. An example approach would be testing whether rock attributes given by the input data sets are consistent with each other and with the labels assigned by the interpreter. This will involve the application of pattern recognition techniques to provide the geological equivalent of a grammar checker.

Acknowledgements

This work was financially supported by Geological Survey of Western Australia (GSWA) in the Royalties for Region Exploration Incentive Scheme, and Australian Research Council Linkage LP140100267. We acknowledge the scientific contribution of Peter Kovesi, Mark Jessell and Mike Dentith, and thank the support of Ian Tyler and Ruth Murdie from GSWA.

References

Aitken, A., Holden, E.J., Dentith, M., 2013. Semi-automated quantification of the influence of data richness on confidence in the geological interpretation of aeromagnetic maps. Geophysics 78 (2), J1–J13.
Blakely, R.J., Simpson, R.W., 1986. Approximating edges of source bodies from magnetic or gravity anomalies. Geophysics v. 51, 1494–1498.
Bond, C.E., Gibbs, A.D., Shipton, Z.K., Jones, S., 2007. What do you think this is? "Conceptual uncertainty" in geoscience interpretation. GSA Today 17 (11), 4.
Cella, F., Fedi, M., Florio, G., 2009. Toward a full multiscale approach to interpret potential fields. Geophys. Prospect. 57, 543–557.
Cooper, G.R.J., Cowan, D.R., 2006. Enhancing potential field data using filters based on the local phase. Comput. Geosci. 32, 1585–1591.
Fedi, M., 2002. Multiscale derivative analysis: a new tool to enhance detection of gravity source boundaries at various scales. Geophys. Res. Lett. 29 (2), 16.1–16.4 1029.
Gonzalez, R.C., Woods, R.E., 2002. Digital Image Processing, 2nded. Prentice-Hall Inc., NUpper Saddle River, NJ, USA, pp 393-404.
Holden, E.J., Dentith, M., Kovesi, P., 2008. Towards the automatic analysis of regional aeromagnetic data to identify regions prospective for gold deposits. Comput.

Geosci. 34 (11), 1505–1513.
Holden, E.J., Dentith, M., Kovesi, P., and Fu, S.C., 2010, CET Grid Analysis Extension, Available from Geosoft ⟨http://www.geosoft.com/pinfo/partners/CET gridanalysis.asp⟩.
Holden, E.J., Wong, J.C., Kovesi, P., Wedge, D., Dentith, M., Bagas, L., 2012. Identifying regions of structural complexity in regional aeromagnetic data for gold exploration: an image analysis approach. Ore Geol. Rev. 46, 47–59.
Hornby, P., Boschetti, F., Horowitz, F., 1999. Analysis of potential field data in the wavelet domain. Geophys. J. Int. 137, 175–196.
Kovesi, P., 1997. Symmetry and asymmetry from local phase. In: Proceedings of the Tenth Australian Joint Converence on Artificial Intelligence, pp. 2–4.
Kovesi, P., 1999. Image features from phase congruency. J. Comput. Vis. Res. 1, 1–26.
Kovesi, P., 2012. Phase preserving tone mapping of non-photographic high dynamic range images. In: Proceedings of the 2012 International Conference on Digital Image Computing: Techniques and Applications (DICTA), 3–5 Dec, pp.1,8.
Kovesi, P.D., Holden, E.J., Wong, J., 2014. Interactive multi-image blending for visualization and interpretation. Comput. Geosci. 72, 147–155.
Lindsay, M.D., Aillères, L., Jessell, M.W., de Kemp, E.A., Betts, P.G., 2012. Locating and quantifying geological uncertainty in three-dimensional models: analysis of the Gippsland Basin, southeastern Australia. Tectonophysics 546–547, 10–27.
Lindsay, M.D., Aitken, A.R., Ford, A., Dentith, M.C., Hollis, J.A., and Tyler, I.M., 2015a, Mineral Prospectivity of the King Leopold Orogen and Lennard Shelf: Analysis of Potential Field Data in the west Kimberley Region. Geological Survey of Western Australia, Report 142, 65 p.
Lindsay, M., Aitken, A., Ford, A., Dentith, M., Hollis, J., Tyler, I., 2015b. Reducing Subjectivity in Multi-commodity Mineral Prospectivity Analyses: Modelling the west Kimberley. Ore Geology Reviews, Australia, in press.
Lindsay, M., Jessell, M.W., Aillères, L., Perrouty, S., de Kemp, E., Betts, P.G., 2013. Geodiversity: exploration of 3D geological model space. Tectonophysics 594, 27–37.
Martin, D.McB., Hocking, R.M., Riganti, A., Tyler, I.M., 2014. 1:500 000 State interpreted bedrock geology of Western Australia, 2014. Digital Data Layer: Geological Survey of Western Australia, ⟨http://www.dmp.wa.gov.au/geoview⟩.
Morlet, J., Arens, G., Fourgear, E., Giard, D., 1982. Wave propagation and sampling theory – part II: sampling theory and complex waves. Geophysics 47 (2), 222–236.
Morrone, M.C., Burr, D.C., 1988. Feature detection in human vision: a phase-dependent energy model. Proc. R. Soc. Lond. B 235, 221–245.
Morrone, M.C., Owens, R.A., 1987. Feature detection from local energy. Pattern Recognit. Lett. 6, 303–313.
Sivarajah, Y., Holden, E.J., Togneri, R., Dentith, M., 2013. Identifying effective interpretation methods for magnetic data by profiling and analysing human data interactions. Interpretation 1 (1), T45–T55.
Sivarajah, Y., Holden, E. J., Togneri, R., Dentith, M. C., Lindsay, M., 2014. Visual saliency and potential field data enhancements: where is your attention drawn? Special Section: Interpretation and Integration of Gravity and Magnetic Data, Interpretation, November, pp. SJ9–SJ21.
Tyler, I.M., Griffin, T.J., 1990. Structural development of the King Leopold Orogen, Kimberley region, Western Australia. J. Struct. Geol. 12 (5–6), 703–714.
Vasuki, Y., Holden, E.J., Kovesi, P.D., Micklethwaite, S., 2014. Semi-automatic mapping of geological structures using UAV-based photogrammetric data: an image analysis approach. Comput. Geosci. 69, 22–32.
Wellmann, J.F., Regenauer-Lieb, K., 2012. Uncertainties have a meaning: information entropy as a quality measure for 3-D geological models. Tectonophysics 526–529, 207–216.